





CARD9 deficiency promotes pancreatic cancer growth by blocking dendritic cell maturation via SLC6A8-mediated creatine transport

Cheng Tian¹, Huimin Yuan¹, Yi Lu², Henghui He³, Qing Li¹, Senlin Li¹, Jian Yang¹, Mengheng Wang¹, Ruochen Xu¹, Qian Liu³, and Ming Xiang¹

¹Department of Pharmacology, School of Pharmacy, Tongji Medical College, Huazhong University of Science and Technology, Wuhan, China; ²State Key Laboratory of Respiratory Disease, The First Affiliated Hospital of Guangzhou Medical University, Guangzhou, China; ³Department of Forensic Medicine, Tongji Medical College, Huazhong University of Science and Technology, Wuhan, China

ABSTRACT

Pancreatic cancer (PC) is featured with low survival rate and poor outcomes. Herein, we found that the expression of caspase-recruitment domain-containing protein 9 (CARD9), predominantly expressed in innate immune cells, was positively related to the prognosis of PC patients. CARD9-deficient PC mice exhibited rapid cancer progression and poorer survival rate. CARD9 knockout decreased dendritic cell (DC) maturation and impaired DC ability to activate T cells *in vivo* and *in vitro*. Adoptive DC transfer confirmed that the role of CARD9 deficiency in PC relied on DCs. Creatine was identified as the most significant differential metabolite between WT DCs and CARD9^{-/-} DCs wherein it played an essential role in maintaining DC maturation and function. CARD9 deficiency led to decreased creatine levels in DCs by inhibiting the transcription of the creatine-specific transporter, solute carrier family 6 member 8 (SLC6A8). Further, CARD9 deletion blocked p65 activation by abolishing the formation of CARD9-BCL10-MALT1 complex, which prevented the binding between p65 and SLC6A8 promoter. These events decreased the creatine transport into DCs, and led to DC immaturity and impairment in antitumor immunity, consequently promoting PC progression.

ARTICLE HISTORY

Received 23 December 2022
Revised 11 April 2023
Accepted 13 April 2023

KEYWORDS

CARD9; creatine; dendritic cells; pancreatic cancer; SLC6A8

Introduction



Pancreatic cancer (PC) is a malignant disease characterized by poor prognosis and high mortality but without an effective treatment¹. Pancreatic tumor cells evade the immune surveillance due to their low immunogenicity and antigenicity, which is attributed to lack of neoantigens and poor antigen presentation². The immunosuppression of PC also results from increased population of immunosuppressive cells along with decreased number of cytotoxic T cells and dendritic cells (DCs)². Hence, immunotherapy based on T cells is only feebly effective for PC treatment³. However, DC vaccination loaded with PC lysate was shown to successfully yield T cell immunity against PC and delay tumor growth⁴.

DCs are cardinal antigen-presenting cells that orchestrate an antitumor immune response by mediating T cell activation and proliferation after tumor antigen stimulation⁵. However, DCs were systemically dysregulated in early-stage PC, which probably led to poor T cell infiltration in tumor foci⁶. Overcoming DC paucity in early PC and restoring DC function in advanced PC ameliorated antitumor immunity and restrained tumor growth⁷. DC vaccination loaded with PC cell lysates increased PC cell apoptosis and CD8⁺ T cell infiltration⁸. Clinical trials based on DC immunotherapy for PC have demonstrated safety, effectiveness, and immune


improvement⁹. DC metabolism regulates its maturation and function¹⁰. In the tumor microenvironment, abnormal metabolites produced by tumor cells alter DC metabolism and impair their functions, thereby resulting in tumor immune escape¹¹. Combination of metabolism regulation and immunotherapy improved the DC function in presenting antigen to T cells and priming them¹².

Caspase-recruitment domain-containing protein 9 (CARD9) is chiefly expressed in innate immune cells, especially macrophages and DCs¹³. As an imperative integrator of the innate immunity, CARD9 mediates signaling from multiple pattern recognition receptors (PRRs) by forming a CARD9/B cell lymphoma/leukemia 10 (BCL10)/mucosa-associated lymphoid tissue lymphoma translocation protein 1 (MALT1) (CBM) complex. Therefore, CARD9 exerts a regulatory effect on a variety of disorders, including infection, cancer, cardiovascular pathologies, inflammatory diseases, and metabolic disorders^{14–17}. Although CARD9 is involved in tumorigenesis, development, or metastasis of numerous cancers such as lung and colon cancers^{18,19}, its exact role in PC remains undefined.

Creatine, an organic acid containing nitrogen, is associated with the progression and metastasis of PC²⁰. It is also implicated in the activation of CD8⁺ T cells and polarization of macrophages^{21,22}. Creatine is mainly synthesized by glycine

CONTACT Ming Xiang  xiangming@tjmu.edu.cn  Department of Pharmacology, School of Pharmacy, Tongji Medical College, Huazhong University of Science and Technology, Hang Kong Road 13, Wuhan 430000, China

[#]These authors contributed equally to this work.

 Supplemental data for this article can be accessed online at <https://doi.org/10.1080/2162402X.2023.2204015>.

© 2023 The Author(s). Published with license by Taylor & Francis Group, LLC.

This is an Open Access article distributed under the terms of the Creative Commons Attribution-NonCommercial License (<http://creativecommons.org/licenses/by-nc/4.0/>), which permits unrestricted non-commercial use, distribution, and reproduction in any medium, provided the original work is properly cited. The terms on which this article has been published allow the posting of the Accepted Manuscript in a repository by the author(s) or with their consent.

amidinotransferase (GATM) and N-guanidinoacetate methyltransferase (GAMT) in the liver and kidney. GATM acts on glycine and L-arginine to produce guanidinoacetate, which is subsequently transformed into creatine by GAMT. Creatine is also transported into cells from circulation through solute carrier family 6 member 8 (SLC6A8), a specific transporter of creatine²², and is subsequently phosphorylated to phosphocreatine. Phosphocreatine is an energy storage metabolite that participates in ATP metabolism and provides energy for energy-consuming cells through the action of creatine kinase²³. Cyclocreatine, a creatine analog, exerted the similar effect as creatine without the transporter SLC6A8²². Cyclocreatine is phosphorylated to cyclocreatine phosphate, which provides energy for cells with high energy demands²⁴.

Herein, we found that CARD9 expression was positively associated with the prognosis of PC patients and that CARD9 deficiency aggravated PC in mice. Multiparametric cytometric techniques showed that CARD9 knockout dramatically decreased intratumoral DC levels and inhibited DC maturation. Metabolomics and RNA sequencing (RNA-seq) revealed that DC maturation downregulation upon CARD9 deletion was mediated through the decrease in creatinine level in DCs. Further, lack of CARD9 prevented the formation of the CBM complex and activation of p65, which suppressed the binding of p65 to SLC6A8 promoter. This event led to a decrease in creatine transportation into DCs, which then were unable to mature and present neoantigens to CD8⁺ T cells and consequently contributed to PC exacerbation.

Materials and methods

Mice

Male wild-type (WT) C57BL/6J mice were procured from Beijing Vital River Laboratory Animal Technology Co. Ltd (Beijing, China), CARD9^{-/-} mice and CD11c-diphtheria toxin receptor (DTR) mice on C57BL/6J background were obtained from Cyagen Biosciences Inc (Suzhou, China) and Shulaibao Biosciences Inc (Wuhan, China), respectively. All mice, fed under specific pathogen-free conditions, were 8 week-old at the beginning of the experiments and were matched for age and sex. All experimental procedures were ethically approved by the Institutional Animal Care and Use Committee of Tongji Medical College.

Cell culture

Murine pancreatic adenocarcinoma cells (Panc02) were acquired from Shanghai Aolu Biological Technology Co. Ltd (Shanghai, China) and cultured in DMEM (HyClone, Logan, UT, USA) supplemented with 10% fetal bovine serum (FBS) and 100 U/mL penicillin-streptomycin (Invitrogen, Carlsbad, CA, USA).

Mouse bone marrow-derived DCs (BMDCs), obtained from the bone marrow of WT or CARD9^{-/-} mice, were incubated in RPMI-1640 medium (HyClone) supplemented with FBS, penicillin-streptomycin, interleukin (IL)-4 (10 ng/mL, PeproTech, Rocky Hill, NJ, USA), and granulocyte macrophage colony-stimulating factor (20 ng/mL,

PeproTech) for 7 days. On day 7, BMDCs were treated with lipopolysaccharide (LPS, 250 ng/mL) and Panc02 tumor lysates for 24 h to induce neoantigen-loaded DCs^{4,8}. In detail, Panc02 cells were collected and resuspended at concentration of 1×10^6 /mL in PBS, which were then freeze-thawed for three times and sonication for 3×10 s with an amplitude of 10 mm to obtain tumor lysates. On day 7, cyclocreatine (MedChemExpress, Shanghai, China) or phosphate-buffered saline (PBS) was added in the culture medium of BMDCs to explore the effect on WT-DCs and CARD9^{-/-} DCs. RGX202 (MedChemExpress) was supplemented in the culture medium of BMDCs 24 h before LPS and Panc02 lysate treatment.

T cells were extracted and isolated from the spleen tissue using CD3⁺ cell isolation kit (Precision BioMedicals, Tianjin, China), which were cultured in RPMI-1640 medium supplemented with FBS and penicillin-streptomycin. In detail, spleen was ground through 40 μ m cell filter to obtain single cell suspension, which was resuspended by ImunoSepTM Buffer and adjusted to 1×10^8 /mL. Following addition of sorting reagent, incubation and centrifugation and other series of operations according to the specification, CD3⁺ T cells were obtained. The purity of CD3⁺ T cells (>90%) was detected using flow cytometry analysis (FigureS1A). CD4⁺ T cell were purified with CD4⁺ T cell isolation kit following the protocol (Precision BioMedicals, Tianjin, China). The CD4⁺ T cells purity was above 90% confirmed by flow cytometry analysis (FigureS1B).

Orthotopic xenograft model of PC and bioluminescence imaging

After mixing with Matrigel (BD Bioscience, San Jose, CA, USA), Panc02 cells (1×10^6) expressing firefly luciferase were injected into the pancreatic cauda to construct an orthotopic xenograft model of PC. Bioluminescence imaging was performed using a Lago X optical imaging system (SI Imaging) to detect the growth of the tumor on day 7, 14, and 21. After an intraperitoneal injection of D-luciferin (150 mg/kg, PerkinElmer, Waltham, MA, USA), mice were anesthetized by 2% vaporized isoflurane and imaged for 10 min. All mice, except those used to assess survival time, were euthanized after 21 days of treatment.

Preparation of single tumor-infiltrating cell suspensions

Tumors were sliced into small fragments and digested by DNase (150 μ g/mL, Sigma, St. Louis, MO, USA) and collagenase IV (1 mg/mL, Sigma) at 37°C for 30 min. Then, digested tumors were smashed to filter through a 70 μ m cell strainer in the presence of PBS.

Flow cytometry analysis

Flow cytometry was performed using a Sony ID7000 (Sony, Tokyo, Japan) or C6 flow cytometer (BD Accuri), and the data were processed via FlowJo 10. Following incubation with CD16/32 (BD Biosciences) on ice for 10 min, samples were stained with fluorochrome-labeled antibody panels on ice for

60 min under dark conditions. For intracellular protein staining, cells were treated with a fixation/permeabilization solution kit before staining. For cytokine staining, monensin (MedChemExpress) was used to block Golgi.

Fluorochrome-labeled antibodies used were as follows: AF700-FVS, APC-CY7-CD45, PE-CY7-CD11b, PE-F4/80, BV605-GR-1, FITC-CD11c, BV480/PE-MHC-II, BV421/APC-CD86, AF647-CD206, FITC-Ly6G, APC-CD3, BV421/FITC-CD4, PERCP/PE-CD8, PE-CY7-NK1.1, APC-CCR7, APC-IFN- γ , AF647-Foxp3, PE-CD25 (BD Biosciences). All of these antibodies were manufactured by BD Biosciences.

Mixed lymphocyte reaction (MLR)

BMDCs subjected to different treatments from different groups of animals and spleen CD3⁺ T cells from WT mice were co-cultured at a ratio of 1:10 for 72 h. The function of CD3⁺ T cells was detected via APC-IFN- γ and PERCP/PE-CD8 staining, and their proliferation was explored using carboxyfluorescein diacetate succinimidyl ester (CFSE, Absin, Shanghai, China) staining. BMDCs from WT or CARD9^{-/-} mice were co-cultured with spleen CD4⁺ T cells from WT mice at a ratio of 1:10 for 24 h or 72 h. Following co-culturing for 72 h, CD4⁺ T cell proliferation was explored using CFSE. BMDCs were removed following co-culturing for 24 h. After 48 h of culture alone, the function of CD4⁺ T cells was explored via detecting the secreted level of cytokines by ELISA assay. In brief, T cell suspension (5×10^5 cells/mL) was stained with 2 μ M CFSE in PBS containing 10% FBS, and maintained at 37°C for 15 min in the dark. Then, stained T cells were washed with PBS containing 10% FBS and subsequently used as CFSE-labeled cells for detecting proliferation of T cells.

Co-culture of T cells with Panc02 and apoptosis analysis

BMDCs subjected to different treatments and spleen CD3⁺ T cells from WT mice were co-cultured at a ratio of 1:10 for 24 h. Subsequently, CD3⁺ T cells were isolated using CD3⁺ cell isolation kit and co-cultured with Panc02 cells at a ratio of 10:1 for 72 h²⁵. Subsequently, the apoptotic rate of Panc02 was detected using Annexin V-PI apoptosis detection kit (Yeasen, Shanghai, China).

DC deletion and adoptive transfer into CD11c-DTR mice

Diphtheria toxin (DT, 6 ng/g body weight, D0564, Sigma) was intraperitoneally injected into CD11c-DTR mice to delete DCs (CD11c⁺) once every 2 days, starting 2 days before tumor inoculation.

The BMDCs from WT and CARD9^{-/-} mice were stimulated with LPS and Panc02 lysate to produce neoantigen-loaded DCs, which were transplanted to CD11c-DTR mice via tail vein injections on day 0, 7, 14, and 21 (5×10^6 cells per mouse).

Quantitative real-time PCR (qPCR)

Total mRNA was extracted using Trizol reagent (Invitrogen) based on instructions of the manufacturer, and reverse transcribed into cDNA using a reverse transcription kit (Promega,

Madison, WI, USA). Green Master Mix was used to carry out qPCR on CFX Connect Real-Time PCR System (Bioer, Hangzhou, China). The mRNA levels were normalized to corresponding *GAPDH* level. The primers used are summarized in Table S1.

Western blot analysis

The extracted proteins were separated via sodium dodecyl sulfate polyacrylamide gel electrophoresis (SDS-PAGE), and the separated bands were transferred onto a polyvinylidene difluoride membrane. Following blocking with 5% bovine serum albumin, the membrane was incubated with primary antibodies for 12 h at 4°C. The primary antibodies were specific for CARD9 (Cell Signaling Technology, Danvers, MA, USA), BCL10, MALT1, p65, phosphorylated p65, glyceraldehyde 3-phosphate dehydrogenase (GAPDH, Bioswamp, Wuhan, China), and SLC6A8 (Proteintech, Wuhan, China). The membrane was subsequently probed with appropriate secondary antibodies to visualize the protein bands. Anti-GAPDH antibody was used as a control.

Immunofluorescence

Immunofluorescence was conducted according to the manufacturer's instructions. BMDCs were incubated with an anti-p65 primary antibody (Cell Signaling Technology), and then stained with a goat anti-rabbit IgG labeled with Andy Fluor™ 488 (Cell Signaling Technology) and 4',6-diamidino-2-phenylindole (DAPI; Sigma). Confocal microscopy (LSM780, Zeiss, Oberkochen, Germany) was performed to obtain cell images.

Untargeted metabolomics

Following LPS and Panc02 lysate or PBS treatment for 24 h, BMDCs were dissolved in an extracting solution (the volume ratio of acetonitrile, methanol, and water was 2:2:1, pre-chilled to -20°C). Each sample (about 5×10^6 BMDCs) was centrifuged at 25,000 rpm for 15 min at 4°C, and the metabolite-containing supernatant was collected and dried using a frozen vacuum concentrator. The dried sample was then dissolved in 200 μ L of a 90% methanol aqueous solution with vortexing for 60 s, sonicated for 10 min, and centrifuged for 15 min. Metabolites were separated and detected using an ultra-pressure liquid chromatography (UPLC) system coupled to a Q-Exactive mass spectrometer (Thermo Fisher Scientific, Waltham, MA, USA). Both positive- and negative-ion modes were used to analyze data. The raw data from liquid chromatography tandem mass spectrometry (LC-MS/MS) were imported into Compound Discoverer 3.1 (Thermo Fisher Scientific) to carry out metabolomic profiling, and the exported files were pretreated with metaX. Subsequently, data quality was evaluated via repeatability of quality control samples. Differential metabolites were screened using multivariable statistics, including principal component analysis (PCA), partial least squares discrimination analysis (PLS-DA), and univariate statistics. Metabolites with significant differences were defined as both $p < 0.05$

using Student's *t*-test and variable importance in projection (VIP) value > 1 via PLS-DA analysis.

RNA-seq

WT-BMDCs and *CARD9*^{-/-} BMDCs were treated with LPS and Panc02 lysates for 24 h, and their RNA was extracted. The purity and integrity of RNA was analyzed, and the MGI system was used to carry out RNA-seq. Fastp was used to treat raw reads to carry out quality control. Clean reads were mapped using Hisat2, and gene quantification and differential expression analysis were performed via RSEM (version 1.3.1) and DESeq2 (version 1.4.5), respectively.

Chromatin immunoprecipitation (ChIP) qPCR assay (ChIP-qPCR)

The ChIP assay was performed to explore the binding of SLC6A8 promoter with p65 via SimpleChIP Plus Enzymatic Chromatin IP Kit (Cell Signaling Technology). Briefly, 1×10^7 BMDCs were crosslinked via formaldehyde after washing twice with PBS, and then lysed using sodium dodecyl sulfate buffer and sonicated. The ChIP dilution buffer was added to the fragmented chromatin, which was incubated with a rabbit anti-p65 antibody for 12 h. Rabbit IgG was used as a negative control, and rabbit anti-histone H3 antibody served as the positive control. After incubation with magnetic beads coated with protein A + G, collected immunoprecipitated products were eluted and digested with proteinase K to acquire DNA. The DNA was purified for RT-qPCR analysis.

Hematoxylin-eosin(HE) staining

The mice were sacrificed, on day 21 following Panc02 cells treatment, to obtain tumor specimens. After fixation with 4% paraformaldehyde, these specimens were embedded in paraffin and sectioned to slices, which were stained with HE.

Bioinformatics and data analysis

The gene expression data of The Cancer Genome Atlas (TCGA)-pancreatic ductal adenocarcinoma (PAAD) and corresponding records of patients were obtained from the University of California Santa Cruz (UCSC) Xena browser, and cases without follow-up records were deleted. The R package was used to explore gene expression in GSE62452, and the National Genomics Data Center (NGDC) database was used to analyze single-cell RNA-seq data from CRA001160.

Survival difference and differentially expressed genes (DEGs) between *CARD9* high and low expression groups were detected using Kaplan-Meier survival analysis and DESeq2 R package (version 1.26.0), respectively. Gene set enrichment analysis (GSEA) was carried out to identify the significantly differential functions and pathways between these two groups via ggplot2 R package (v 3.6.2). The data with significant difference were identified with an adjusted *p*-value < 0.05, normalized enrichment score > 1, and a false discovery rate < 0.25. Gene Ontology (GO) and Kyoto

Encyclopedia of Genes and Genomes (KEGG) were used to analyze DEGs using “clusterProfiler” package.

Statistical analysis

The results are shown as the mean ± standard error of mean (SEM). Student's *t* test was used to analyze the significance in *CARD9* expression of PC patients in tumor or paratumor tissues, Log-rank test in survival curve of PC patients based *CARD9* expression, Breslow test in survival curve of PC mice, Mann-Whitney U test in two groups (*n* = 5 or 6), Kruskal-Wallis test in three groups (*n* = 6), and Dunn test in subgroups of two groups. A value of *p* < 0.05 denoted significance (**p* < 0.05, ***p* < 0.01, ****p* < 0.001).

Results

CARD9 deficiency aggravated PC

The Gene Expression Omnibus (GEO) database revealed that *CARD9* expression was downregulated in tumor tissues from PC patients as compared with that in adjacent paratumor tissues (Figure 1A). Survival analysis conducted based on TCGA database revealed the positive association between *CARD9* expression and overall survival of PC patients (Figure 1B). These results demonstrated that *CARD9* potentially exerted an antitumor effect on PC. To verify this hypothesis, we constructed *CARD9*-knockout (KO) mice and explored the role of *CARD9* in PC (Fig. S1C-F).

***p* < 0.01.

CARD9^{-/-} and normal mice were orthotopically transplanted with luciferase-labeled Panc02 cells, and live images were acquired on day 7, 14, and 21 after tumor implantation. Mice were later sacrificed and their tumor tissues were harvested (Figure 1C). *CARD9* deletion led to a decrease in the survival rate of PC mice (Figure 1D). The tumor volume gradually increased with time, and was larger for *CARD9*^{-/-} mice than for normal mice (Figure 1E, F). The loss in body weight was higher and the spleen index was lower in *CARD9*^{-/-} mice than in normal mice (Fig. S2A, B). Hematoxylin and eosin (HE) staining showed that *CARD9* deficiency exacerbated the damage to the pancreas and promoted tumor proliferation (Figure 1G). qPCR results showed that the transcription of antitumor cytokines, including tumor necrosis factor- α (*TNF- α*), interferon- γ (*IFN- γ*), *IL-1 β* , *IL-12*, greatly decreased and the expression of protumor cytokines such as *IL-10* and *TGF- β* clearly increased in *CARD9*^{-/-} mice (Figure 1H). Thus, *CARD9* exerts an antitumor effect on PC.

CARD9 deficiency decreased proportion, maturity, and function of DCs in PC mice

Given that *CARD9* is mainly expressed in innate immune cells, we speculated that *CARD9* might mitigate PC by activating an antitumor immunity. mRNA levels of all genes in PC patients based on *CARD9* expression were compared via KEGG and GO database. Compared to PC patients with low *CARD9* expression, those with high *CARD9* expression showed significant alteration in expression of multiple genes. Functional

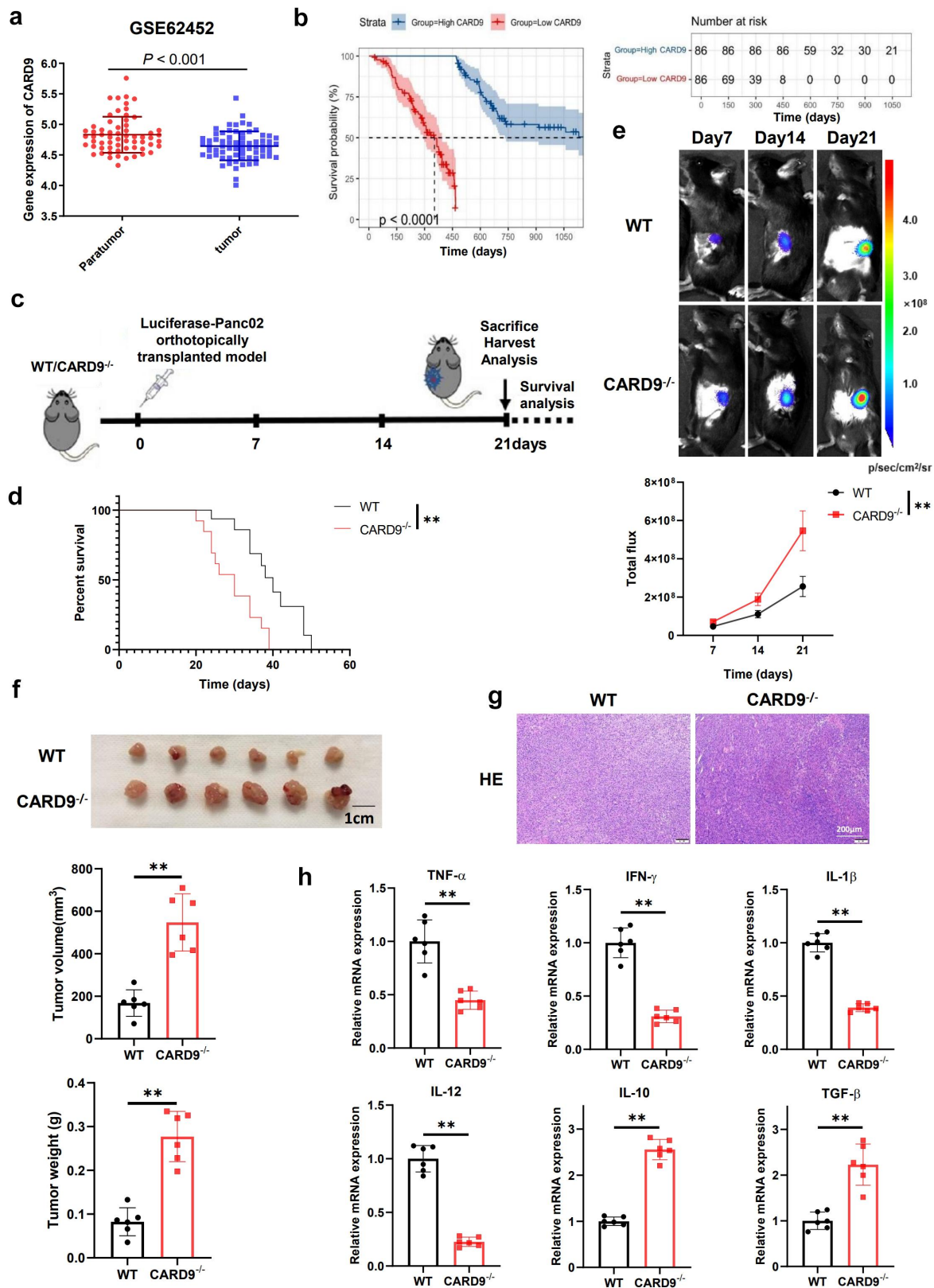


Figure 1. CARD9 deficiency aggravated PC. (A) the expression of CARD9 in the paratumor and tumor tissues of PC patients based on GEO database. (B) the association of CARD9 level with overall survival of PC patients according to TCGA database. (C) Schematic diagram of the animal experiment. (D) Overall survival of WT and CARD9^{-/-} mice with PC ($n=24$). (E) Bioluminescence imaging of PC and quantitative analysis. (F) Image of tumors and graphs of tumor volume and weight. (G) HE staining of tumor tissue. (H) Transcriptional levels of inflammatory cytokines in the tumor tissue. (E-H) Data expressed as mean \pm SD ($n=6$). ** $p < 0.01$.

enrichment analysis displayed the top 20 differential signaling pathways, which showed that the CARD9-mediated regulation

of PC was strongly intertwined with immunity (Fig. S3A), which is consistent with our speculation. Therefore, we

compared the immune cells in the tumor foci from WT and CARD9^{-/-} mice using multiparametric cytometric techniques (Fig. S4). CARD9 deficiency significantly reduced the proportions of M1 and M2 macrophages, especially myeloid DCs, and enhanced the proportion of MDSCs in the tumor (Figure 2A, B). Lymphocyte analysis showed that CARD9^{-/-} mice had lower levels of CD8⁺ T, CD4⁺ T, NK, and NKT cells in the tumor (Figure 2C, D). Besides, CARD9 deficiency inhibited DC maturity and decreased CD4⁺ T and CD8⁺ T cells in the spleen and lymph node (Fig. S5A, B). Therefore, CARD9 knockout could exacerbate PC by affecting DC maturity and function, which might be the reason for lymphocyte alteration.

To ascertain our speculation, we compared the maturation and function of BMDCs with or without CARD9 *in vitro*. CARD9 deficiency decreased the levels of CCR7, CD86, MHCII and suppressed antitumor cytokines, IL-1 β , TNF- α , IL-6 and IL-12 (Figure 2E-G, S5C). It also inhibited BMDC-induced CD8⁺ T cell increase and its IFN- γ production, as well as proliferation of T cells (Figure 2H,I), along with suppressed proliferation and activation of CD4⁺ T cells and promoted differentiation to Tregs (Fig. S5D-F). Single cell expression profile matrix for CRA001160 also confirmed that CARD9 alleviated PC by affecting the functions of immune cells, especially DCs (Fig. S3B), and CARD9 expression positively correlated with DC maturation markers (Fig. S3C), which is in line with our results. Thus, CARD9 deficiency mainly inhibited proportion, maturity, and function of DCs in PC mice.

CARD9 deficiency exacerbated PC through DC immaturity and dysfunction

Based on the *in vivo* results and bioinformatics data, we speculated that the CARD9-mediated regulation of PC was dependent on DCs. Therefore, we constructed a CD11c-DTR mouse deprived of DCs and compared its PC severity with the WT mouse (Fig. S6). CD11c-DTR and WT mice were orthotopically transplanted with luciferase-labeled Panc02 cells (Fig. S7A). In comparison with WT mice, CD11c-DTR mice had shorter survival, slower tumor progression, and smaller tumor size (Fig. S7B-D). HE staining result showed that the tumor tissue of CD11c-DTR mice developed more severe lesion (Fig. S7E). Flow cytometry analysis revealed the decrease in the proportion of CD8⁺ T and CD4⁺ T cells in the tumor of DC-depleted mice (Fig. S7F). qPCR results showed that DC depletion led to a decrease in the expression of antitumor cytokines, including TNF- α , IFN- γ , IL-1 β , and IL-12, and an increase in the expression of pro-tumor cytokines such as IL-10 and TGF- β (Fig. S7G). These results manifested that DCs exerted a beneficial effect by inhibiting PC development.

To avoid the influence of endogenous DCs, we adoptively transferred BMDCs from WT and CARD9^{-/-} mice to CD11c-DTR mice by tail vein injection (Figure 3A). In comparison with the PBS treatment group, WT BMDC transfer showed diminished tumors, increased survival rate, enhanced proportion of CD8⁺ T and CD4⁺ T cells, and changes in the expression of inflammatory cytokines in the tumor. Compared with WT BMDC transfer, however, CARD9^{-/-} BMDC transfer promoted tumor progression, decreased survival rate, downregulated CD8⁺ T and CD4⁺ T cells, and induced pro-tumor

microenvironment (Figure 3B-G). As a consequence, the CARD9-mediated alleviation in PC relied on DCs.

CARD9 deficiency blocked DC maturation by decreasing cellular creatine level

The maturity of DCs was reported to be associated with its metabolism²⁶, and CARD9 was involved in regulation of metabolism of immune cells²⁷. To investigate whether the CARD9-mediated regulation of metabolism was involved in DC maturity, we detected the metabolites of WT and CARD9^{-/-} BMDCs treated with LPS (5 μ g/mL) and Panc02 lysate for 24 h by metabolomic analysis. PLS-DA was used to identify the differential metabolites between WT and CARD9^{-/-} BMDCs. The scores of the principle component 1 (PC1) were 29.89% and 23.11% in negative-ion and positive-ion mode, respectively (Fig. S8A). The results showed several differential metabolites between WT and CARD9^{-/-} BMDCs, and arginine and proline metabolism was the most significant differential metabolic pathway (Figure 4A,B). We also analyzed the differential metabolites belonging to arginine and proline metabolism, and found that the absence of CARD9 dramatically decreased L-arginine, L-proline, and creatine levels in DCs (Figure 4C). To verify the result of metabolomics, we determined the level of creatine, the most obvious differential metabolite, in BMDCs. CARD9 deficiency led to a decrease in the intracellular level but an increase in the extracellular level of creatine (Figure 4D).

To explore the main resource of creatine in BMDCs, we detected the expression of creatine synthesis-associated proteins, GATM and GAMT, and the creatine transporter SLC6A8, and observed that the expression of SLC6A8 was the highest (Figure 4E). Besides, the SLC6A8 inhibitor RGX202 markedly downregulated the cellular level but upregulated the extracellular level of creatine in BMDCs (Figure 4F). Therefore, creatine in BMDCs was principally derived from extracellular transport via SLC6A8, and RGX202 was used to investigate the role of creatine in BMDC maturity and function. Cellular creatine decrease caused by RGX202 led to blockade of BMDC maturation induced by LPS and Panc02 lysate, including lower levels of MHCII, CD86, and CCR7, as well as inhibited production of TNF- α , IL-1 β , IL-6, and IL-12 in DCs (Figure 4G-H, S8B). It also contributed to dysfunctional BMDCs, which failed to induce CD8⁺ T cell increase and its IFN- γ production as well as proliferation of T cells, and inhibited Panc02 apoptosis induced by T cells (Figure 4I-J, S8C). Thus, creatine played a pivotal role in DC activation, and lack of CARD9 expression led to reduced cellular creatine level and the consequent blockade of DC maturity.

CARD9 knockout decreased creatine transport via blockade of SLC6A8 expression

To explore how CARD9 deficiency arrested creatine level in BMDCs, we detected the expression of genes encoding creatine-associated proteins, including GATM, GAMT, CKB, and SLC6A8, by RNA-seq (Figure 5A). The results showed that

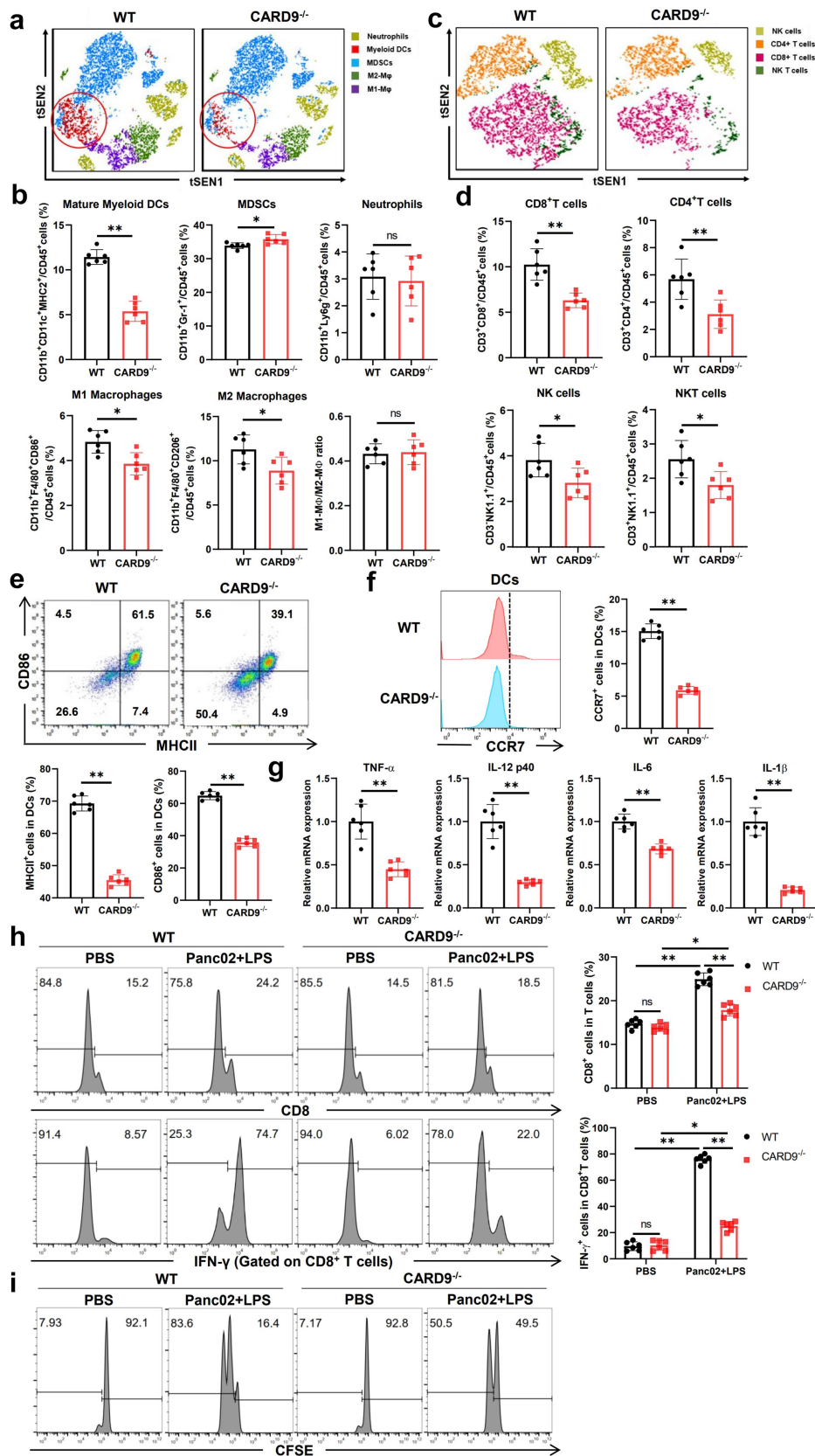


Figure 2. CARD9 manipulated the enrichment, maturity, and function of DCs. (A-B) Innate immune cells in the tumor foci from PC mice, as analyzed by multiparametric cytometry. (C-D) Lymphocytes in the tumor foci from PC mice, as analyzed by multiparametric cytometry. (E) MHCII and CD86 levels in BMDCs after stimulation with LPS and Panc02 neoantigen. (F) CCR7 levels in BMDCs. (G) Transcriptional levels of cytokines in BMDCs. (H) CD8 levels in T cells and IFN- γ levels in CD8⁺ T cells co-cultured with BMDCs from WT and CARD9^{-/-} mice. (I) Proliferation of T cells co-cultured with BMDCs from WT and CARD9^{-/-} mice determined using CFSE staining. Data expressed as mean \pm SD ($n=6$). * $p<0.05$, ** $p<0.01$, ns: no significance.

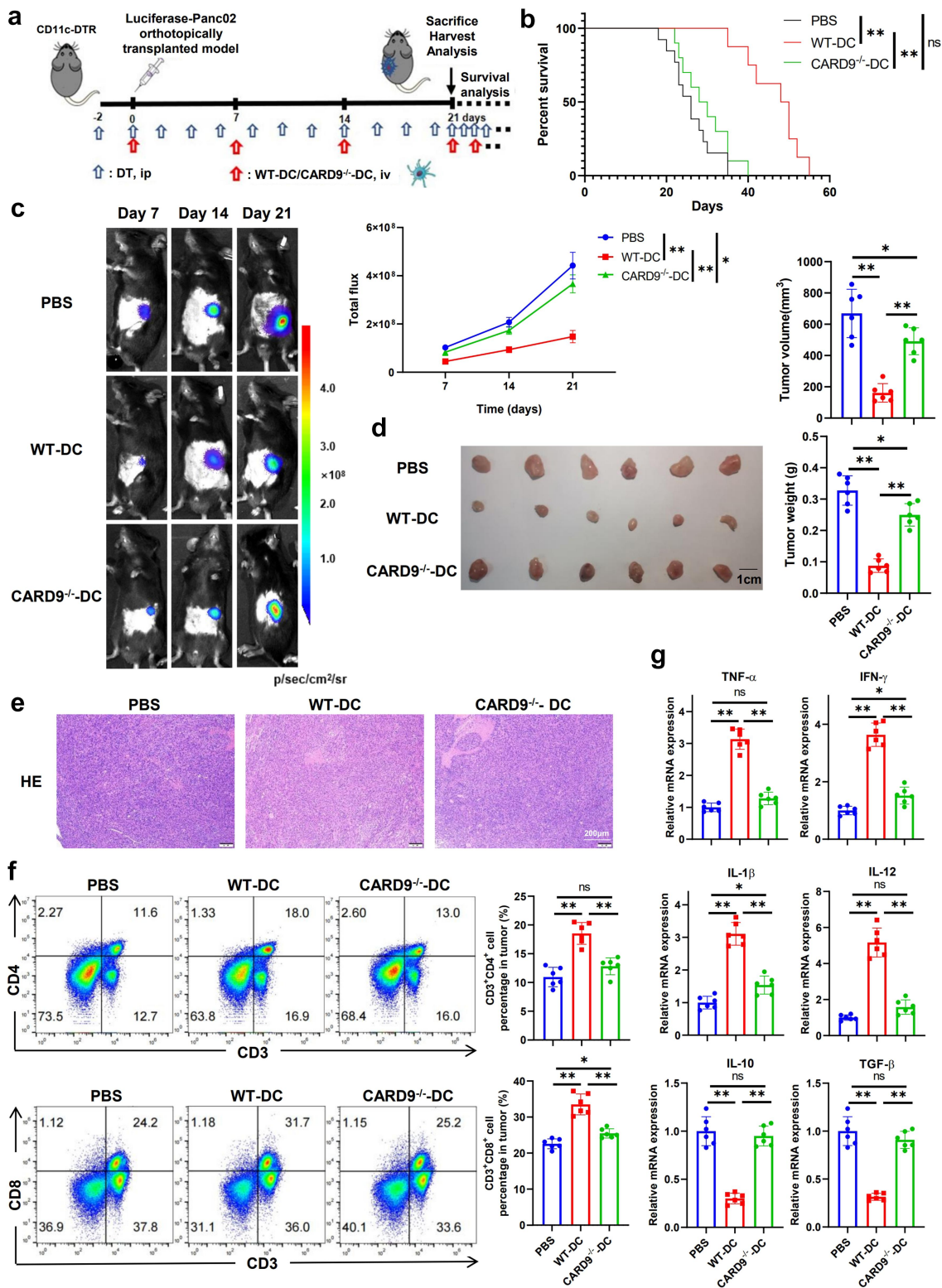


Figure 3. CARD9 was essential for mediating an effective antitumor response by DCs. (A) Schematic diagram of the animal experiment. (B) Overall survival of CD11c-DTR mice treated with PBS, WT DCs, or CARD9^{-/-} DCs ($n=24$). (C) Bioluminescence imaging of PC and quantitative analysis. (D) Image of tumors and graphs of tumor volume and weight. (E) HE staining of PC. (F) Percentage of CD8⁺ T and CD4⁺ T cells in PC foci. (G) Transcriptional levels of inflammatory cytokines in the tumor tissue. (C-G) Data expressed as mean \pm SD ($n=6$). * $p<0.05$, ** $p<0.01$, ns: no significance.

CARD9 deficiency inhibited the transcription of *SLC6A8* but had no effect on the expression of *GATM*, *GAMT* and *CKB*, which is consistent with qPCR results (Figure 5B,C). Western blotting result also showed that CARD9 deficiency decreased the protein level of *SLC6A8* (Figure 5D). Therefore, *SLC6A8*

downregulation was presumably associated with the decrease in creatine level owing to CARD9 deficiency.

Subsequently, we treated WT and CARD9^{-/-} BMDCs with PBS, creatine, or cyclocreatine. As the effect of creatine is similar to that of cyclocreatine which is transported into the cell

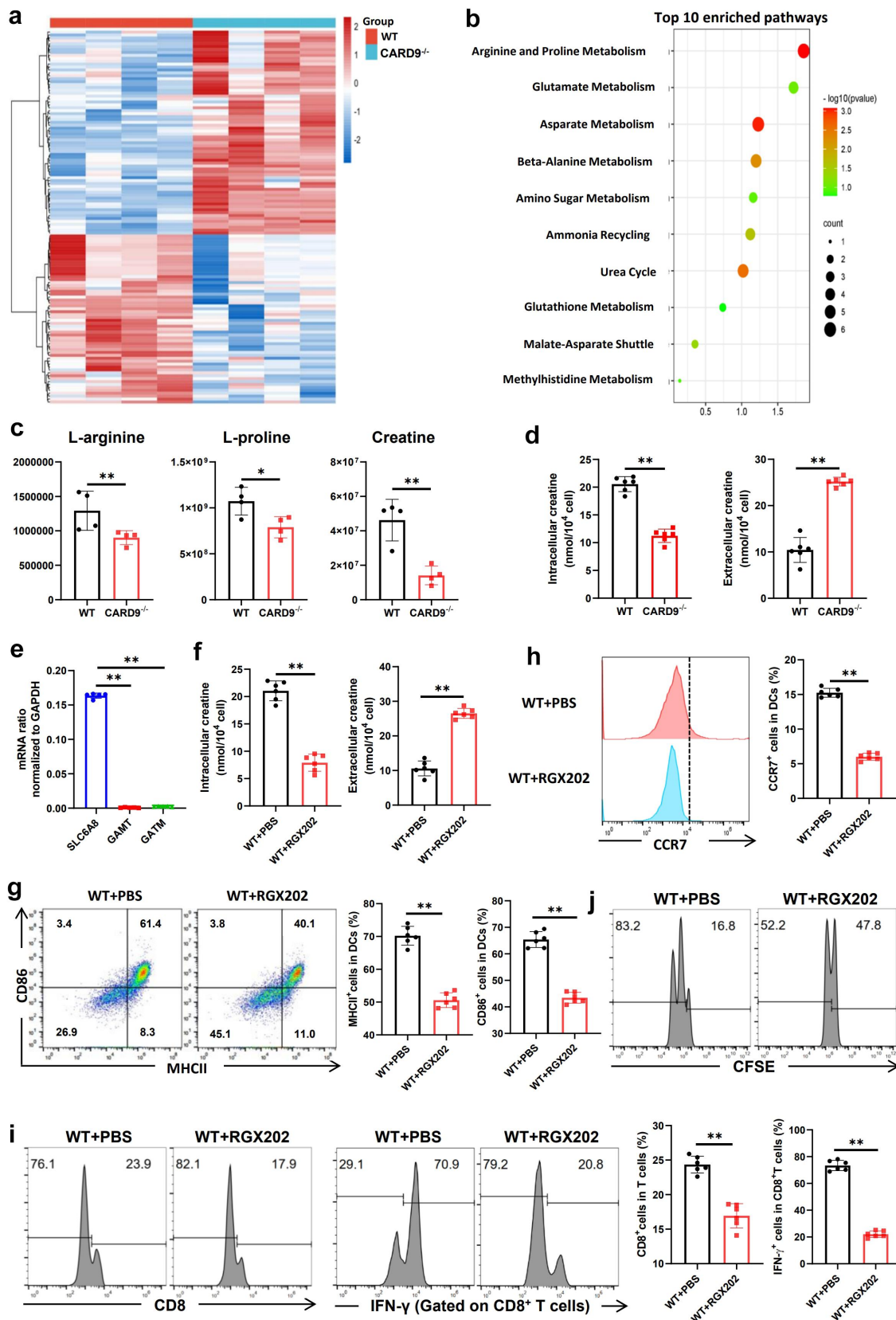


Figure 4. CARD9 deficiency blocked DC maturity by decreasing cellular creatine levels. BMDCs from WT and *CARD9*^{-/-} mice were treated with LPS and Panc02 lysate. (A) Differential metabolites between WT and *CARD9*^{-/-} BMDCs via metabolomics (*n*=4). (B) Top 10 differential metabolic pathways between WT and *CARD9*^{-/-} BMDCs. (C) Levels of L-arginine, L-proline, and creatine in BMDCs (*n*=4). (D) Intracellular and extracellular levels of creatine in BMDCs (*n*=6). (E) mRNA levels of SLC6A8, GATM, and GATM in BMDCs, as determined by qPCR (*n*=6). (F) Intracellular and extracellular creatine levels in WT BMDCs treated with PBS or RGX202 (*n*=6). (G) MHCII and CD86 levels in BMDCs (*n*=6). (H) CCR7 levels in BMDCs (*n*=6). (I) CD8 levels in T cells and IFN- γ levels in CD8⁺ T cells co-cultured with BMDCs (*n*=6). (J) Proliferation of T cells co-cultured with BMDCs determined by CFSE staining. Data expressed as mean \pm SD. **p*<0.05, ***p*<0.01.

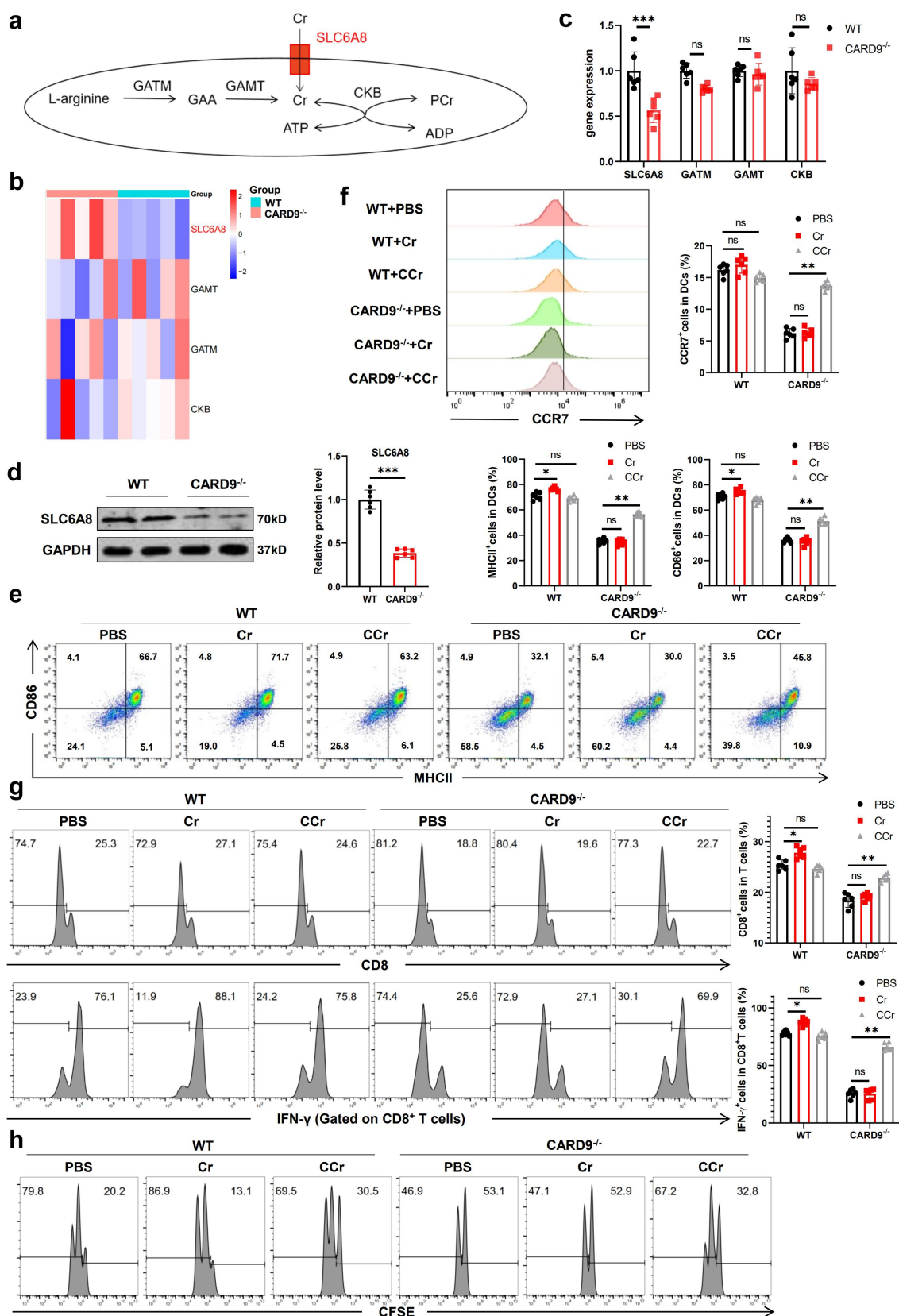


Figure 5. CARD9 knockout reduced the transport of creatine by blocking SLC6A8 expression. (A) the schematic chart of cellular creatine resource. (B) mRNA levels of creatine-associated proteins, including SLC6A8, GATM, GAT, and CKB in BMDCs as determined by transcriptomics ($n=5$). (C) Relative mRNA levels of SLC6A8, GATM, GAT, and CKB in BMDCs as determined by qPCR ($n=6$). (D) SLC6A8 protein level in BMDCs ($n=6$). (E) MHCII and CD86 levels in BMDCs treated with PBS, creatine (Cr), or cyclocreatine (CCr). (F) CCR7 level in BMDCs ($n=6$). (G) CD8 levels in T cells and IFN- γ levels in CD8 $^+$ T cells co-cultured with BMDCs ($n=6$). (H) Proliferation of T cells co-cultured with BMDCs via CFSE. Data expressed as mean \pm SD. * $p < 0.05$, ** $p < 0.01$, ns: no significance.

independent of SLC6A8, we supplemented the WT and CARD9^{-/-} BMDCs with creatine or cyclocreatine. Creatine increased the levels of MHCII, CD86, TNF- α , and IL-6 on WT BMDCs, which showed a slight increase in T cell proliferation and cytotoxicity, including augmented IFN- γ production and CD8⁺ T cell proportion as well as Panc02 apoptosis. However, creatine exhibited no effect on CARD9^{-/-} BMDCs. Cyclocreatine saliently upregulated levels of CD86, MHCII, CCR7 and anti-tumor cytokines in CARD9^{-/-} BMDCs, and prominently enhanced their function of activating T cells (Figure 5E-H, S8D-E). Cyclocreatine, but not creatine, reversed the immaturity and dysfunction of CARD9^{-/-} BMDCs, indicating that creatine analog acting independent of SLC6A8 alleviated BMDC immaturity caused by CARD9 deficiency, while creatine that

acted in a SLC6A8-dependent manner exhibited no such effect. Taken together, SLC6A8 downregulation led to CARD9 depletion-mediated creatine insufficiency and impairment in DC maturity and function.

CARD9 knockout inhibited SLC6A8 transcription by downregulating the CARD9/BCL10/MALT1-p65 pathway

As CARD9 deficiency downregulated SLC6A8 transcription, we hypothesized that CARD9 knockout altered the activation of transcription factors (TFs). Thus, we converged predicted TFs of SLC6A8 with those affected by CARD9 deficiency based on transcriptomic data, and chose five TFs, namely, USF2, NFI, ELK1, IRF1, and p65/NF- κ B (Figure. 6A). p65 was the only TF whose expression was associated with SLC6A8 expression (Figure. 6B,

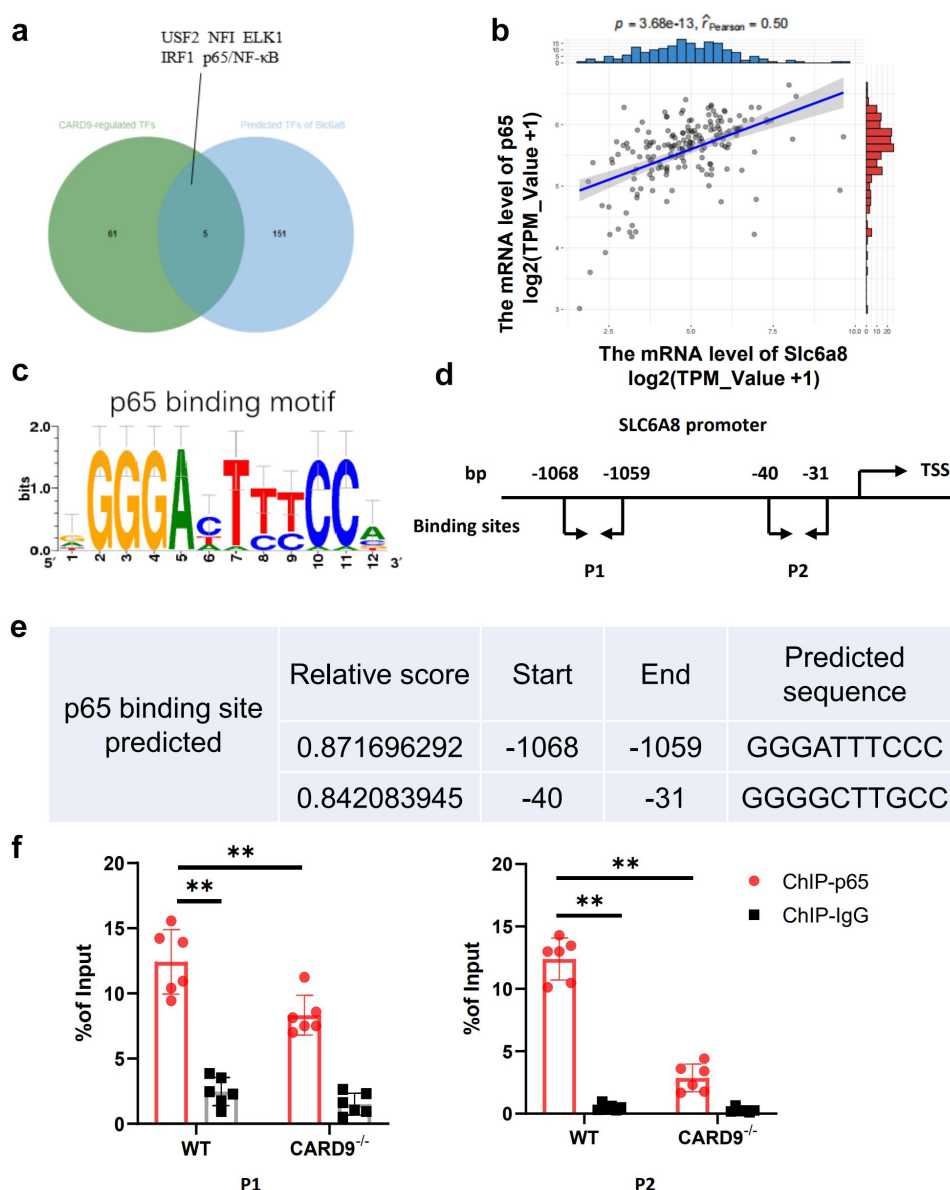


Figure 6. CARD9 knockout inhibited SLC6A8 transcription by decreasing the binding of p65 to SLC6A8 promoter. (A) the merger of transcription factors affected by CARD9 deficiency and the predicted transcription factors of SLC6A8. (B) the association of p65 with SLC6A8 transcription. (C-E) Predicted SLC6A8 promoter-binding site for p65. (F) Binding results of p65 with SLC6A8 promoter in BMDCs from WT and CARD9^{-/-} mice using ChIP. Data expressed as mean \pm SD ($n=6$).** $p<0.01$.

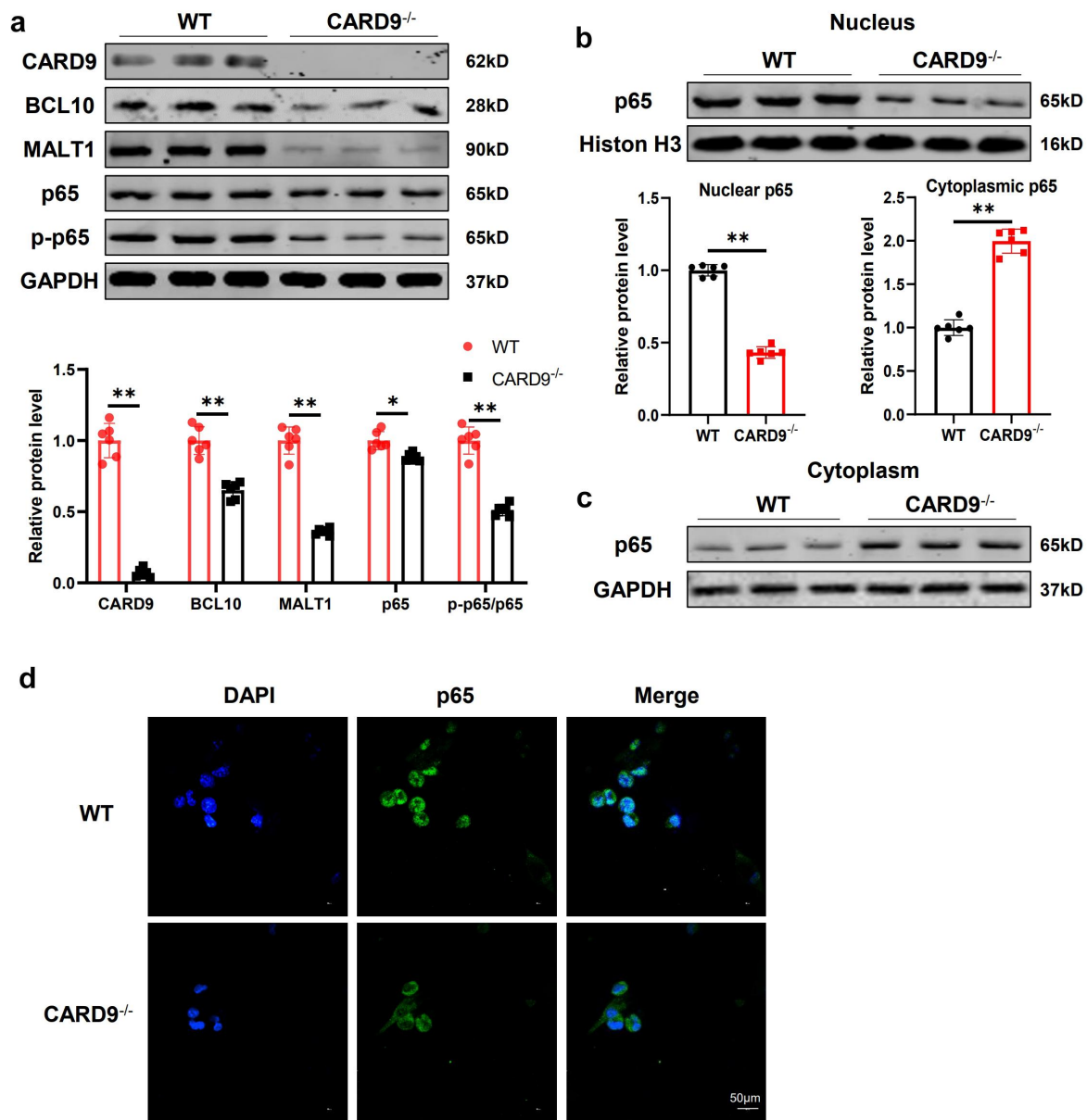


Figure 7. CARD9 deficiency restrained the activation and nuclear transportation of p65 by repressing the formation of the BCM complex. (A) Protein levels of CARD9, BCL10, MALT1, p65, and phosphorylated p65. (B) Nuclear protein level of p65. (C) Cytoplasmic protein level of p65. (D) Immunofluorescence of p65 (green) in DCs. Data expressed as mean \pm SD ($n=6$). * $p<0.05$, ** $p<0.01$.

S9). As a classical downstream molecule of CARD9, p65 regulates the transcription of SLC6A8²². To explore whether p65 plays a pivotal role in SCL6A8 downregulation caused by CARD9 deficiency, we used the ChIP assay to detect the binding of p65 to the promoter of SLC6A8 in WT and CARD9^{-/-} BMDCs (Figure 6C-E). The binding of p65 to SLC6A8 promoter considerably decreased in CARD9^{-/-} BMDCs compared with that in WT BMDCs (Figure 6F).

We detected the classical pathway of CARD9. CARD9 deletion decreased the expression of BCL10, MALT1, and p65 and the phosphorylation of p65 (Figure 7A), consistent with the decrease in the nuclear expression and augmentation in the cytoplasmic level of p65 (Figure 7B-D). Thus, CARD9 deletion inhibited p65 activation and nuclear transfer, which prevented the binding between p65 and SLC6A8 promoter. These events

led to a decrease in the expression of SLC6A8 and the consequent inhibition of creatine transfer into BMDCs.

Discussion

This study describes a heretofore unidentified effect of CARD9 deficiency on DC-mediated antitumor immune responses in PC through the CBM-p65-SLC6A8-creatine axis. CARD9 expression was higher in PC tumor tissue than in the paratumoral tissue, and positively correlated with the overall survival of PC patients. Therefore, we speculated that CARD9 was involved in blocking PC progression. We verified this hypothesis in CARD9^{-/-} mice where CARD9 deficiency aggravated PC and decreased their survival.

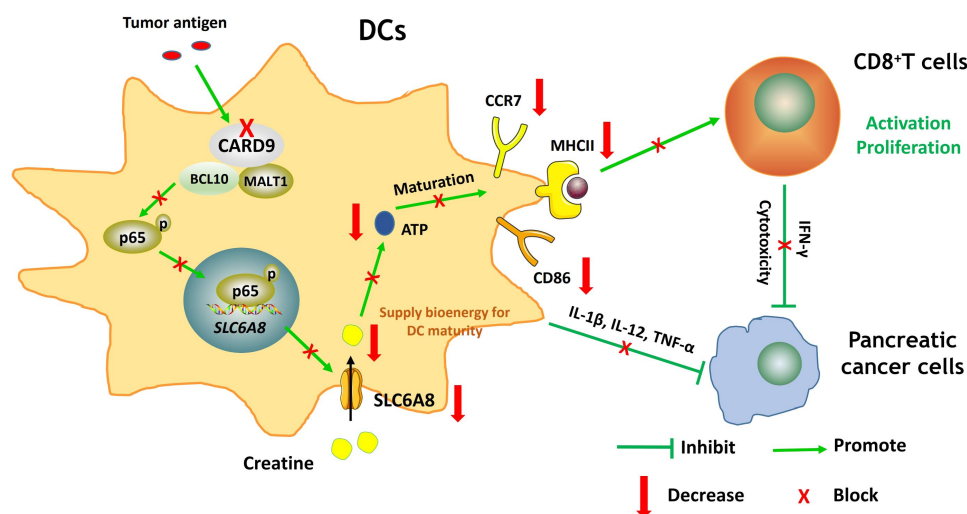


Figure 8. A schematic diagram depicting CARD9-p65-SLC6A8-creatine pathway-mediated DC maturation and the interaction between DCs, CD8⁺ T cells, and pancreatic cancer cells.

As CARD9 is mainly expressed in myeloid cells, we used multiparametric cytometric techniques to explore the main cells affected by CARD9. Our results demonstrated that CARD9 deficiency overtly induced DC immaturity and decreased the lymphocyte proportion in tumor foci. CARD9 deficiency also led to the production of naïve DCs *in vitro*. As classical APCs, DCs present neoantigens to lymphocytes and induce antitumor immune responses²⁸, and DC dysregulation is one of the main reasons underlying immune surveillance evasion in PC²⁹. These findings indicate that the CARD9 scarcity-mediated DC immaturity might result in lymphocyte diminishment and PC exacerbation. To corroborate the vital role of DCs in PC, we constructed CD11c-DTR mice deprived of DCs, which developed more severe PC. We also transferred WT BMDCs and CARD9^{-/-} BMDCs into CD11c-DTR mice, which averted the interference of endogenous DCs, to prove that DC immaturity mediated by CARD9 paucity caused PC aggravation. However, typical activated macrophages (M1 type) also expressed CD11c, and CD11c ablation decreased the population of M1 type macrophages. This might be one of reasons why CD11c deletion aggravated PC. Nevertheless, neoantigen-loaded WT BMDCs were more effective against PC in CD11c-DTR mice than PBS or CARD9^{-/-} BMDCs, which validates our postulation.

The activation and function of DCs are associated with metabolism^{11,30}, and we, therefore, used metabolomics to detect the differential metabolites between WT and CARD9^{-/-} BMDCs. The results showed that CARD9 depletion altered multiple metabolic pathways, particularly arginine and proline metabolism, in which creatine was the most prominent differential metabolite. Creatine exerted an indispensable effect on activation of CD8⁺ T cells and polarization of macrophages^{21,22}. Therefore, we speculated that creatine was the key metabolite mediating the CARD9 deficiency-induced BMDC dysfunction. Given that creatine in BMDCs is mainly derived from transportation, we decreased cellular creatine level using a creatine transporter inhibitor. Creatine shortage inhibited the maturity and function of BMDCs, which is consistent with our speculation. CARD9 deficiency and creatine deprivation decreased ATP levels in BMDCs,

while cyclocreatine treatment remarkably restored cellular ATP levels (Fig. S10). Creatine affected the function of CD8⁺ T cells by maintaining intracellular energy²¹. In addition, cyclocreatine is phosphorylated by CKB to cyclocreatine phosphate, which also serves as a reservoir of energy²⁴. Therefore, one might presume that creatine controlled DC maturation by providing energy.

However, creatine increased maturation in WT DCs, while cyclocreatine showed no effect on WT DCs. That might be due to their different structure stability. Cyclocreatine and creatine are phosphorylated into phosphocyclocreatine and phosphocreatine respectively, both of which provide energy for cells via dephosphorylation, by creatine kinase^{23,31}. Phosphocyclocreatine is structurally similar to phosphocreatine, while much difficult to be reversely catalyzed to release ATP on account of the distinct kinetic and thermodynamic properties²³. Therefore, cyclocreatine supplement resulted in more phosphocyclocreatine and less phosphocreatine. The reason why cyclocreatine does not increase maturation in WT DCs in our study might be that the energy provided by increased phosphocyclocreatine is counteracted by decreased phosphocreatine.

RNA-seq and qPCR results also unveiled that SLC6A8 was the most significantly altered creatine-related proteins, and WT BMDCs and CARD9^{-/-} BMDCs exhibited similar maturation and functions after SLC6A8 inhibitor (RGX202) treatment (Data not shown). Cyclocreatine, able to be transported into cell without SLC6A8, but not creatine restored BMDC maturation and function in the context of CARD9 scarcity. These results substantiated our surmise that CARD9 deficiency inhibited SLC6A8 expression and creatine transport into DCs, which terminated in DC immaturity and dysfunction.

Furtherly, as RNA-seq and qPCR results shown, CARD9 deletion suppressed SLC6A8 transcription. We analyzed potential SLC6A8-associated TFs and those altered by CARD9 knockout. Five TFs, including USF2, NFI, ELK1, IRF1, and p65, were potentially involved in SLC6A8 expression regulation and were affected by CARD9. Further analysis unveiled p65 as the only TF associated with SLC6A8 expression. ChIP

results showed that CARD9 deficiency hindered the binding of p65 to SLC6A8 promoter, and western blotting and immunofluorescence confirmed that CARD9 knockout abolished the formation of the CBM complex and the subsequent activation of p65, which prevented p65 transportation into the nucleus. As a key factor mediating DC maturation, however, p65 is also capable of binding to promoter of inflammatory cytokines, including TNF- α , IL-1 and IL-6, and promoting DC maturity^{32,33}. That might be one of the reasons why cyclocreatine is unable to counteract completely the effect of CARD9 deficiency on DC maturity. Therefore, the interaction between p65 and inflammatory cytokines might be also involved in DC immaturation induced by CARD9 deficiency.

Collectively, CARD9 deficiency abrogated the formation of the CBM complex, suppressed p65 phosphorylation and activation, blocked p65 binding to SLC6A8 promoter, and down-regulated SLC6A8 expression, which gave rise to inadequate creatine transfer into DCs. Creatine shortage culminated in immature and dysfunctional DCs, which failed to present neoantigens to CD8⁺ T cells. This dysregulation blunted the cytotoxic effect of CD8⁺ T cells on PC and aggravated PC (Figure 8).

Author contributions

Ming Xiang participated in the study design, material support, coordination, and supervision of the study. Cheng Tian, Huimin Yuan, and Yi Lu designed the experimental validation, performed experiments, analyzed the data, and drafted the manuscript. Henghui He, Qing Li, Senlin Li, Jian Yang, Mengheng Wang, and Ruochen Xu carried out parts of the experiments and provided constructive discussion about experiments. Qian Liu provided effective work direction. All authors read and approved the final manuscript.

Disclosure statement

No potential conflict of interest was reported by the authors.

Funding

The work was supported by the National Natural Science Foundation of China [81872000].

ORCID

Cheng Tian  <http://orcid.org/0000-0003-4046-2288>
Ming Xiang  <http://orcid.org/0000-0002-3048-3897>

Data availability statement

The data that support the findings of this study are available from M. X. upon reasonable request.

Ethics approval and consent to participate

Animal care and experimental procedures were carried out in accord with the guidelines of the National Institutes of Health Guide for the Care and Use of Laboratory Animals.

References

- Da Y, Liu Y, Hu Y, Liu W, Ma J, Lu N, Zhang C, Zhang C. STING agonist cGAMP enhances anti-tumor activity of CAR-NK cells against pancreatic cancer. *OncoImmunology*. 2022;21(1):2054105. doi:10.1080/2162402X.2022.2054105.
- Li X, Gulati M, Larson AC, Solheim JC, Jain M, Kumar S, Batra SK. Immune checkpoint blockade in pancreatic cancer: trudging through the immune desert. *Semin Cancer Biol*. 2022;86:14–27. doi:10.1016/j.semcancer.2022.08.009.
- O'Donnell JS, Teng MWL, Smyth MJ. Cancer immunoeediting and resistance to T cell-based immunotherapy. *Nat Rev Clin Oncol*. 2019;16(3):151–167. doi:10.1038/s41571-018-0142-8.
- Lau SP, van Montfoort N, Kinderman P, Lukkes M, Klaase L, van Nimwegen M, van Gulijk M, Dumas J, Mustafa DAM, Lievens SLA, et al. Dendritic cell vaccination and CD40-agonist combination therapy licenses T cell-dependent antitumor immunity in a pancreatic carcinoma murine model. *J ImmunoTher Cancer*. 2020;8(2):e000772. doi:10.1136/jitc-2020-000772.
- Yang J, Shangguan J, Eresen A, Li Y, Wang J, Zhang Z. Dendritic cells in pancreatic cancer immunotherapy: vaccines and combination immunotherapies. *Pathol Res Pract*. 2019;215(12):152691. doi:10.1016/j.prp.2019.152691.
- Lin JH, Huffman AP, Wattenberg MM, Walter DM, Carpenter EL, Feldser DM, Beatty GL, Furth EE, Vonderheide RH. Type 1 conventional dendritic cells are systemically dysregulated early in pancreatic carcinogenesis. *J Exp Med*. 2020;217(8):e20200816. doi:10.1084/jem.20190673.
- Hegde S, Krisnawan VE, Herzog BH, Zuo C, Breden MA, Knolhoff BL, Hogg GD, Tang JP, Baer JM, Mpoy C, et al. Dendritic cell paucity leads to dysfunctional immune surveillance in pancreatic cancer. *Cancer Cell*. 2020;37(3):289–307. doi:10.1016/j.ccell.2020.02.008.
- Shangguan A, Shang N, Figini M, Pan L, Yang J, Ma Q, Hu S, Eresen A, Sun C, Wang B, et al. Prophylactic dendritic cell vaccination controls pancreatic cancer growth in a mouse model. *Cytotherapy*. 2020;2(1):6–15. doi:10.1016/j.jcyt.2019.12.001.
- Lau SP, Klaase L, Vink M, Dumas J, Bezemer K, van Krimpen A, van der Breggen R, Wismans LV, Doukas M, de Koning W, et al. Autologous dendritic cells pulsed with allogeneic tumour cell lysate induce tumour-reactive T-cell responses in patients with pancreatic cancer: a phase I study. *Eur J Cancer*. 2022;169:20–31. doi:10.1016/j.ejca.2022.03.015.
- Giovanelli P, Sandoval TA, Cubillos-Ruiz JR. Dendritic cell metabolism and function in tumors. *Trends Immunol*. 2019;40(8):699–718. doi:10.1016/j.it.2019.06.004.
- Peng X, He Y, Huang J, Tao Y, Liu S. Metabolism of dendritic cells in tumor microenvironment: for immunotherapy. *Front Immunol*. 2021;12:613492. doi:10.3389/fimmu.2021.613492.
- Ray A, Song Y, Du T, Tai Y-T, Chauhan D, Anderson KC. Targeting tryptophan catabolic kynurenine pathway enhances antitumor immunity and cytotoxicity in multiple myeloma. *Leukemia*. 2020;34(2):567–577. doi:10.1038/s41375-019-0558-x.
- Liu X, Jiang B, Hao H, Liu Z. CARD9 signaling, inflammation, and diseases. *Front Immunol*. 2022;13:880879. doi:10.3389/fimmu.2022.880879.
- Jeantin L, Plu I, Amador MDM, Maillart E, Lanternier F, Pourcher V, Davy V. Pearls & Oysters: spinal cord candidiasis linked to CARD9 deficiency masquerading as a longitudinally extensive transverse myelitis. *Neurology*. 2022;99(11):475–479. doi:10.1212/WNL.0000000000200992.
- Zhong X, Chen B, Yang L, Yang Z. Card9 as a critical regulator of tumor development. *Cancer Lett*. 2019;451:150–155. doi:10.1016/j.canlet.2019.03.001.
- Zhang H, Wang Y, Men H, Zhou W, Zhou S, Liu Q, Cai L. CARD9 regulation and its role in cardiovascular diseases. *Int J Biol Sci*. 2022;18(3):970–982. doi:10.7150/ijbs.65979.
- Tian C, Tuo YL, Lu Y, Xu C-R, Xiang M. The role of CARD9 in metabolic diseases. *Curr Med Sci*. 2020;40(2):199–205. doi:10.1007/s11596-020-2166-4.

18. Qu J, Liu L, Xu Q, Ren J, Xu Z, Dou H, Shen S, Hou Y, Mou Y, Wang T. CARD9 prevents lung cancer development by suppressing the expansion of myeloid-derived suppressor cells and IDO production. *Int J Cancer*. 2019;145(8):2225–2237. doi:10.1002/ijc.32355.
19. Malik A, Sharma D, Malireddi RKS, Guy CS, Chang T-C, Olsen SR, Neale G, Vogel P, Kanneganti T-D. SYK-CARD9 signaling axis promotes gut fungi-mediated inflammasome activation to restrict colitis and colon cancer. *Immunity*. 2018;49(3):515–530. doi:10.1016/j.immuni.2018.08.024.
20. Loo JM, Scherl A, Nguyen A, Man F, Weinberg E, Zeng Z, Saltz L, Paty P, Tavazoe S. Extracellular metabolic energetics can promote cancer progression. *Cell*. 2015;160(3):393–406. doi:10.1016/j.cell.2014.12.018.
21. Di Biase S, Ma X, Wang X, Yu J, Wang Y-C, Smith DJ, Zhou Y, Li Z, Kim YJ, Clarke N, et al. Creatine uptake regulates CD8 T cell antitumor immunity. *J Exp Med*. 2019;216(12):2869–2882. doi:10.1084/jem.20182044.
22. Ji L, Zhao X, Zhang B, Kang L, Song W, Zhao B, Xie W, Chen L, Hu X. Slc6a8-mediated creatine uptake and accumulation reprogram macrophage polarization via regulating cytokine responses. *Immunity*. 2019;51(2):272–284. doi:10.1016/j.immuni.2019.06.007.
23. Zhang L, Bu P. The two sides of creatine in cancer. *Trends Cell Biol*. 2022;32(5):380–390. doi:10.1016/j.tcb.2021.11.004.
24. Elgebaly SA, Todd R, Kreutzer DL, Christenson R, El-Khazragy N, Arafa RK, Rabie MA, Mohamed AF, Ahmed LA, El Sayed NS. Nourin-associated miRNAs: novel inflammatory monitoring markers for cyclocreatine phosphate therapy in heart failure. *Int J Mol Sci*. 2021;22(7):3575. doi:10.3390/ijms22073575.
25. Munisvaradass R, Kumar S, Govindasamy C, Alnumair K, Mok P. Human CD3⁺ T-Cells with the Anti-ERBB2 chimeric antigen receptor exhibit efficient targeting and induce apoptosis in erbb2 overexpressing breast cancer cells. *Int J Mol Sci*. 2017;18(9):1797. doi:10.3390/ijms18091797.
26. Yan L, Tan Y, Chen G, Fan J, Zhang J. Harnessing metabolic reprogramming to improve cancer immunotherapy. *Int J Mol Sci*. 2021;22(19):10268. doi:10.3390/ijms221910268.
27. Li DD, Jawale CV, Zhou C, Lin L, Trevejo-Nunez GJ, Rahman SA, Mullet SJ, Das J, Wendell SG, Delgoffe GM, et al. Fungal sensing enhances neutrophil metabolic fitness by regulating antifungal Glut1 activity. *Cell Host & Microbe*. 2022;30(4):530–544. doi:10.1016/j.chom.2022.02.017.
28. Plesca I, Benesova I, Beer C, Sommer U, Müller L, Wehner R, Heiduk M, Aust D, Baretton G, Bachmann MP, et al. Clinical significance of tumor-infiltrating conventional and plasmacytoid dendritic cells in pancreatic ductal adenocarcinoma. *Cancers*. 2022;14(5):1216. doi:10.3390/cancers14051216.
29. Meyer MA, Baer JM, Knolhoff BL, Nywening TM, Panni RZ, Su X, Weilbaecher KN, Hawkins WG, Ma C, Fields RC, et al. Breast and pancreatic cancer interrupt IRF8-dependent dendritic cell development to overcome immune surveillance. *Nat Commun*. 2018;9(1):1250. doi:10.1038/s41467-018-03600-6.
30. Li J, Ding H, Meng Y, Li G, Fu Q, Guo Q, Yin Z, Ye Z, Zhou H, Shen N. Taurine metabolism aggravates the progression of lupus by promoting the function of plasmacytoid dendritic cells. *Arthritis Rheumatol*. 2020;72(12):2106–2117. doi:10.1002/art.41419.
31. Ulland TK, Song WM, Huang SC, Ulrich JD, Sergushichev A, Beatty WL, Loboda AA, Zhou Y, Cairns NJ, Kambal A, et al. TREM2 maintains microglial metabolic fitness in alzheimer's disease. *Cell*. 2017;170(4):649–663. doi:10.1016/j.cell.2017.07.023.
32. Zhao H, Wu L, Yan G, Chen Y, Zhou M, Wu Y, Li Y. Inflammation and tumor progression: signaling pathways and targeted intervention. *Signal Transduct Target Ther*. 2021 Jul 12;6(1):263. doi:10.1038/s41392-021-00658-5.
33. Zeidi M, Kim HJ, Werth VP. Increased myeloid dendritic cells and TNF- α expression predicts poor response to hydroxychloroquine in cutaneous lupus erythematosus. *J Invest Dermatol*. 2019;139(2):324–332. doi:10.1016/j.jid.2018.07.041.